# Impact of Porosity and Electrolyte Composition on the Surface Charge of Hydroxyapatite Biomaterials

Montserrat Espanol,[1,2] Gemma Mestres,[3] Thomas Luxbacher,[4] Jean-Baptiste Dory[1] and Maria-Pau Ginebra[1,2]

[1]Biomaterials, Biomechanics and Tissue Engineering Group, Department of Materials Science and Metallurgical Engineering, Technical University of Catalonia (UPC), Av. Diagonal 647, 08028 Barcelona, Spain

[2]Centre for Research in Nanoengineering, Technical University of Catalonia (CRNE-UPC), Pascual i Vila 15, 08028 Barcelona, Spain

[3]Department of Engineering Sciences, Uppsala University, Box 534, 751 21 Uppsala, Sweden

[4]Anton Paar GmbH, Graz, Austria

**KEYWORDS**

Surface charge, zeta potential, Streaming current, porosity, texture, hydroxyapatite, bone substitute ion adsorption

**ABSTRACT**

The success or failure of a material when implanted in the body is greatly determined by the surface properties of the material and the host tissue reactions. The very first event that takes place after implantation is the interaction of soluble ions, molecules and proteins from the biological environment with the material surface leading to the formation of an adsorbed protein layer that will later influence cell attachment. In this context, the particular topography and surface charge of a material become critical as they influence the nature of the proteins that will adsorb. However, very limited information is available on the surface charge of porous substrates. Only until very recently the determination of the zeta potential on porous membranes has been accurately determined. The goal of this work was to implement the previous findings for the determination of the zeta potential of a series of porous hydroxyapatite (HA) substrates and to assess how porosity affects the measurements. In addition, studies using various electrolytes were also performed to prove how the specific affinity of certain ions for HA can further impact surface charge. The results showed that all materials exhibited very similar external surface charge (~ -23 mV), consistent with their almost identical topographies. However, the presence of interconnected pores underneath the sample surface resulted in an additional internal zeta potential that varied with the porosity content. Measurements with different electrolytes confirmed the selectivity of divalent ions for HA underlying the importance of testing biomaterials using relevant electrolytes.

## 1 INTRODUCTION

*In vitro* and *in vivo* studies have identified nanoscale and microscale features of biomaterials as key modulators of cellular behavior making them a powerful tool in the design of cell instructive biomaterials.[1–3] Cells of typically tens of microns in diameter, with filopodia with diameters in the nanorange, are known to interact with the micro- and nano- features present on the surface of biomaterials, influencing cell adhesion and cellular function.[1,4] However, interaction never occurs directly with the bare surface of the material but through the protein layer that immediately adsorbs on the materials' surface upon implantation.[5] The composition, relative concentration, orientation and conformation of the adsorbed proteins are also features that will definitively influence cell behavior.[6,7] In general it is difficult to discriminate if the cells directly respond to surface topography or they indirectly react to the nature of the adsorbed protein layer. In this already complex scenario, besides the possible influence of topography on protein adsorption by sieving large proteins off or concentrating smaller proteins favoring their adsorption, the chemistry of the underlying material actively participates in the selection of the adsorbed proteins.

Among the wide range of biomaterials used for bone regeneration, hydroxyapatite (HA) with close resemblance to the mineral phase of bone, has long been recognized as an excellent bone substitute owing to its biocompatibility, osteoconductive properties and bioactivity. Although hydroxyapatite has very well-known affinity for proteins –as proved from the wide use of chromatographic HA columns for protein separation-[8–10], the selectivity in protein adsorption is greatly determined by the surface charge that HA develops in the physiological environment. The hexagonal crystallographic system in which biological hydroxyapatite is believed to

crystallize, i.e. P63/m, has two main associated crystallographic faces with notably different surface charge. Prismatic *ac* and *bc* planes with predominance of Ca ions are positively charged surfaces (Ca-sites) while basal *ab* planes through the presence of phosphate groups (P-sites) and hydroxide ions are negatively charged.[8,11] The work by Kandori *et al.* put forward, through systematic protein adsorption studies on hydroxyapatite particles of increasing length, the preferential adsorption of acidic proteins on Ca rich *ac, bc* crystal surfaces and that of basic lysozyme on *ab* surfaces rich in P-sites.[11] Similar conclusions were later confirmed by Zhuang *et al*.[12]

From a different perspective, but in line with the importance of electrical charges, Baxter *et al.* studied polarized HA substrates.[13] The application of an electric field on HA at high temperature (> 200$^{o}$C) is believed to cause migration of protons in the columnar (OH) channels of hexagonal unit cell in HA or the alignment of the hydroxyl groups resulting in surfaces with net negative and positive charges. Although there are contradicting results concerning which type of surface, either positively or negatively charged, have a better influence on cell behavior, it is clear that polarized surfaces can induce different cell behavior when compared to non-polarized ones.[14–16] It is believed that the surface charges built by polarization encourage ion and protein binding of essential constituents on the surface of the biomaterial needed for cell attachment and growth.[16] Ohgaki *et al.* justified an observed greater cell growth on negatively polarized surfaces by the adsorption of Ca and the subsequent attraction of cell adhesion proteins, such as integrins, fibronectin, and osteonectin, which show divalent cation-dependent ligand binding. Upon anchoring of cell adhesion proteins, cell adhesion would follow. On the contrary, they reasoned that the adsorption of negative anions on positively polarized surfaces acted as antiadhesive cues, minimizing cell adhesion.[16]

The importance of surface charge has also been put forward in the design of nanoparticles (NPs) for cell internalization purposes (e.g. drug delivery or gene therapy). Many studies have observed that positively charged NPs can be internalized to a greater extent than negatively charged NPs and this has been explained by the electrostatic affinity between the negative charge on the cell membrane and the positively charged NPs.[17–19]

Although there are many examples supporting the important role of surface charge in mediating/controlling cellular events, this greatly contrasts with the limited available data reporting such values on bulk solid surfaces. Unlike for the case of colloidal systems, the surface charge of solid surfaces has hardly been reported, mainly because commercial instruments only became available in the late 1980s. Moreover, recent advances in the determination of the surface charge of membranes for filtration purposes have put forward that measurements in porous materials could have been misinterpreted if the contribution of the pores to the streaming current was not considered. It has not been till 2010 that Yaroshchuk and Luxbacher provided appropriate formulas to accurately characterize the surface charge of porous samples.[20]

The importance of both porosity and surface charge in the design of bulk biomaterials for bone regeneration applications, together with the lack of studies in the field has motivated the present work. For this purpose biomimetic hydroxyapatite substrates with controlled micro and nanoporosity have been thoroughly characterized in terms of surface charge (zeta potential). In addition, different electrolytes have been used in the measurements to account for the specific interaction of relevant ions present in the biological environment with the material surface.

## 2 MATERIALS AND METHODS

### 2.1 Preparation and characterization of biomimetic hydroxyapatite surfaces

Hydroxyapatite substrates were prepared via a cementitious reaction by mixing a liquid phase consisting of 2.5 w/v % of $Na_2HPO_4$ (Panreac, 131679.1211) with α-tricalcium phosphate powder (α-$Ca(PO_4)_3$, α-TCP) as solid phase.

The α-TCP was in-house made by solid state reaction of calcium hydrogen phosphate ($CaHPO_4$, Sigma C7263) and calcium carbonate ($CaCO_3$, Sigma–Aldrich, C4830) mixed at a 2:1 molar ratio. Both reagents were mixed for 15 min in a mixer (Whip Mix, US) before submitting them to thermal treatment. The treatment was carried out in a furnace (Hobersal CNR-58) set at 1400 $^0$C for 15 h in air. After treatment the powder was quenched in air to stabilise the alpha phase. α-TCP powder was prepared by milling 150 g of powder in a planetary ball mill (Pulverisette 6, Fritsch, Germany) with 10 agate balls (30 mm diameter) for 15 min at 450 rpm, resulting in a median diameter of 5.2 μm. The powder phase was completed by adding 2 wt% of precipitated hydroxyapatite (Merck, 1.02143) as a seed in the powder.

To obtain substrates with different porosities, cements (C) with different liquid to powder ratios (L/P) were prepared: 0.35, 0.45 and 0.55 $mL \cdot g^{-1}$. The liquid and the solid phase were mixed in a speed mixer (DAC 150.1 FV-K, Flack Tek, Landrum, USA) at 2500 rpm for 30 s, and the resulting paste was cast between Teflon sheets separated 1.2 mm apart with the help of glass holders. Approximately after 1h, when the paste had enough cohesion, the Teflon molds were immersed in Milli Q water (18 MΩ·cm, Q-POD from Millipore) and kept at 37 $^o$C for at least 4 days to allow completion of the setting reaction:

$3\alpha\text{-}Ca(PO_4)_3 + H_2O \rightarrow Ca_9(HPO_4)\,(PO_4)_5(OH)$

Characterization of the samples comprised of Scanning Electron Microscopy (SEM) observation to assess the surface morphology of the various materials. Prior to observation

samples were Au/Pd coated to minimize charging effects. Analysis of porosity content and pore size distribution was carried out by mercury intrusion porosimetry (MIP, Autopore IV Micromeritics).

## 2.2 Zeta potential measurements

### *2.2.1 Theory*

Surface charge refers to the charge that spontaneously develops on materials as the result of their reaction in solution (i.e. ionization of functional groups, ion adsorption, etc.). Although strictly speaking surface charge cannot be experimentally measured, the most meaningful and measurable parameter to best describe the charging behaviour at interfaces is the zeta potential ($\zeta$). Once a material comes into contact e.g. with an aqueous solution, ions from the solution immediately adsorb onto the material surface in an attempt to neutralize the material intrinsic charge. Part of these ions tightly bind to the material surface and are considered as immobile ions (Stern layer) and the ones further away, i.e. adsorbed on top of the Stern layer, are regarded as the mobile ones (diffuse layer). Following this model of the electrochemical double layer (EDL), the zeta potential refers to the charge at the interface between these two layers.

In spite that the calculation of zeta potential dates back to the 19$^{th}$ century, the experimental determination of the zeta potential on bulk surfaces has experienced many advances only in the last years. One of the typical measuring configurations consists in the tangential measurement of the streaming potential/current, which is generated by forcing a liquid to flow in the channel between two flat samples that are facing each other.[21–25] This flow pulls the charges of the diffuse layer, generating a potential/current that relates to the zeta potential through the well-known equation derived by von Helmholz and von Smoluchowski (Eq. 1):

$$\zeta\,(I_{str}) = \frac{dI_{str}}{d\Delta p} \cdot \frac{\eta}{\varepsilon \cdot \varepsilon_0} \cdot \frac{L}{A} \qquad \text{Eq.1}$$

Where $I_{str}$ is the streaming current, $\frac{dI_{str}}{d\Delta p}$ is the measured streaming current coefficient, L is the length of the channel formed by the two flat surfaces facing each other and A is its cross-section, A=W·H, W being the channel width and H the channel gap height; η and ε are the viscosity and dielectric coefficient of the electrolyte solution respectively, and $\varepsilon_0$ is the vacuum permittivity.

Although used with great success, this formula implicitly assumes that the material has impermeable walls i.e., it is non-porous. The problem with porous samples, with open pore structures, arises because part of the fluid that is forced in between the two samples travels also through the porous material generating a "parasite" current/potential that adds to that of the channel, masking the results.[24,26,27] In this case, Eq.1 no longer holds, and it should be replaced by the equation proposed in 2010 by Yaroschuck and Luxbacher[20] (Eq. 2).

$$I_{str}^{tot} = I_{str}^{C} + I_{str}^{P} = \frac{\varepsilon \cdot \varepsilon_0}{\eta} \cdot \frac{W}{L} \cdot \Delta p \cdot (H \cdot \zeta_{external} + 2H_P \cdot \gamma \cdot \zeta_{internal}) \qquad \text{Eq. 2}$$

rearranging,

$$\frac{dI_{str}^{tot}}{d\Delta p} = \frac{\varepsilon \cdot \varepsilon_0}{\eta} \cdot \frac{W}{L} \cdot (H \cdot \zeta_{external} + 2H_P \cdot \gamma \cdot \zeta_{internal}) \qquad \text{Eq. 3}$$

where $I_{str}^{C}$ and $I_{str}^{P}$ are the streaming currents generated within the channel and inside the porous structure respectively, H is the gap height (channel height), $H_P$ the thickness of the porous sample, $\gamma$ the porosity of the sample and $\zeta_{internal}$ and $\zeta_{external}$ the effective zeta potential of the inner pore structure and the external surface, respectively.

The contributions of $I_{str}^{C}$ and $I_{str}^{P}$ translate into two independent zeta potentials, an external zeta potential that describes the material surface charge and an internal zeta potential that

accounts for the charge within the inner porous structure. Thus, the so-called "parasite" current in porous structures represents an internal zeta potential by itself.[20,22,27]

In spite of the complexity that adds the incorporation of the internal zeta potential in Eq. 3, the equation can be easily solved owing to the linear dependence between the streaming current coefficient ($\frac{dI_{str}}{d\Delta p}$) and the gap height ($H$). Thus, performing analysis at different gap heights (Eq. 3) results in a linear relationship that allows one to determine separately the contributions of the external surface (slope of the linear fit) from that of its porous structure (offset value).[20]

### *2.2.2 Measuring procedure*

A SurPASS electrokinetic analyzer (Anton Paar GmbH) was used to perform zeta potential analyses by means of streaming current measurements at various distances (gap heights) between adjacent sample surfaces.

Preparation of the samples was carried out without drying the material in the following way. At least 4 days after cement setting, the flat samples were transferred into petri dishes containing enough Milli Q water (18 MΩ·cm, Q-POD from Millipore) to maintain wet the surfaces that had to be measured, while allowing to gently wipe the opposite surfaces which were glued onto a couple of 20 x 10 $mm^2$ holders (Super Glue-3, Loctite). A surgical blade was then used to make a superficial cut on the borders of the sample that exceeded the holder dimensions to help breaking the excess of material. The samples were then mounted in the adjustable-gap cell. A micrometric screw was used to manually adjust the distance between both sample surfaces to the desired gap height (H). Typically, measurements were performed at various gaps in the range of 80-120 μm to ensure well-developed laminar flows, a prerequisite indispensable for channel height determination.[28]

Prior to the measurement, 500 mL of 0.001 M KCl (Panreac, 131494.1210) solution freshly prepared with conductivity ~150 $\mu S \cdot cm^{-1}$ and pH=6 ± 0.3, was circulated through the channel for sufficiently long time (typically between 15-45 min) to allow for sample equilibration. The conductivity, temperature and pH value of the electrolyte solution was continuously monitored. The slope and offset values in Eq. 3 were obtained by streaming the electrolyte solution across the channel gap (i.e., measuring $\frac{dI_{str}}{d\Delta p}$ at different gap heights). This was achieved by increasing the pressure linearly from 0 to 300 mbar in alternating directions. Measurements were done with a pair of Ag/AgCl electrodes with a nominal surface area sufficiently large to minimize any electrode polarization during measurement -the alternating flow also helped minimizing polarization-. In addition, cell conductance data were also obtained at each gap from electrical resistance measurements using the same pair of electrodes.

**Figure 1** summarizes in four graphs the most significant information obtained from tangential flow measurements used in the present work. **Figure 1A** shows the linear dependence between volume flow rate and pressure difference at a fixed gap height. From this linear dependence and applying the Hagen-Poiseuille relation it was determined the gap height.[20] **Figure 1B** shows the variation of streaming current with pressure difference at different gap heights in alternating flow directions. The slope for each curve is represented in **Figure 1C** as a function of gap height. The streaming current coefficients for this linear dependence i.e., offset and slope, are essential to determine the internal and external zeta potential values respectively (Eq. 3). In **Figure 1D** conductance is plotted against gap height. In this case, the offset and slope of the linear fit correspond to pore conductance and electrolyte conductivity (the slope is half the value of the conductivity), respectively.

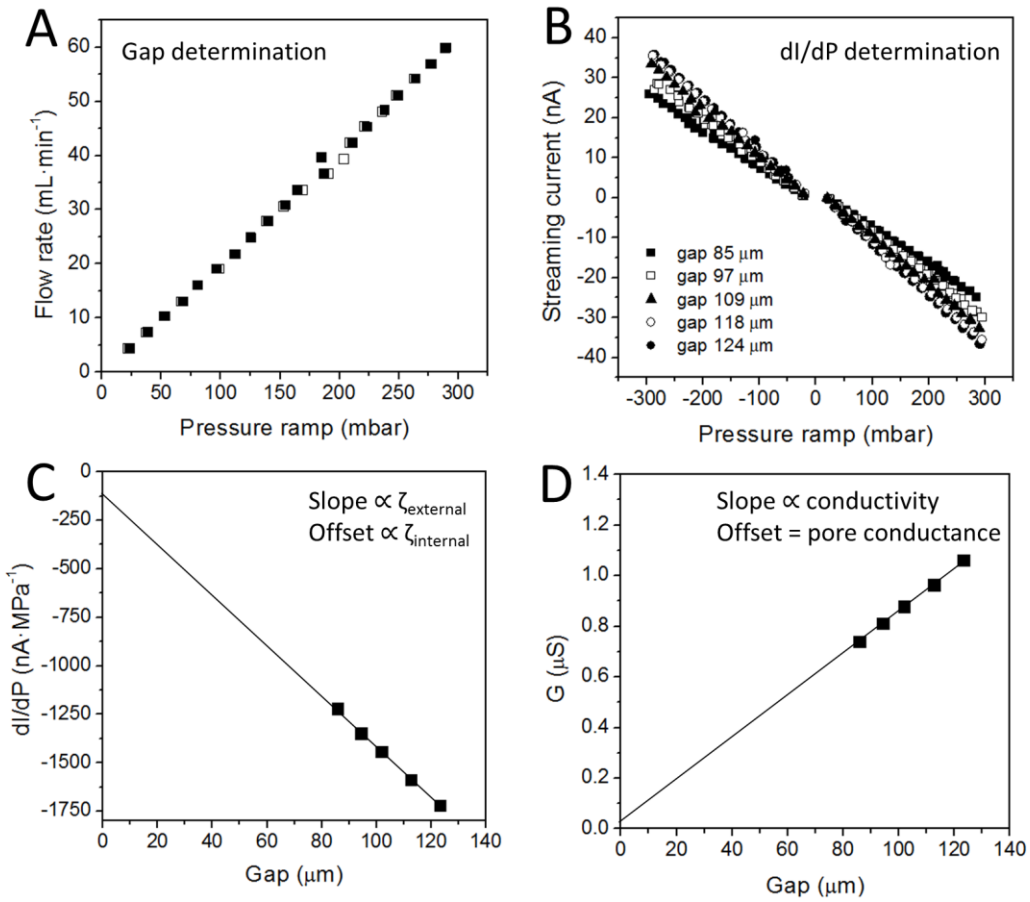


**Figure 1**. Typical graphs obtained from tangential streaming current measurements showing: (a) linear dependence between flow rate and pressure ramp, (b) variation of streaming current with pressure difference at different gap heights in alternating flow directions, (c) the slope of each ramp from (b) is represented versus gap height, and (d) plot of cell conductance against gap height.

To ensure quality of all measured samples the following aspects had to be fulfilled:

- Linear dependences of streaming current and volume flow on the differential pressure (**Figure 1A and B**).
- Close values for the offset and slope coefficients in the two flow directions (**Figure1B**).

- Correspondence between measured and calculated electrical conductivity. The former was monitored throughout the experiment using a conductometer while the latter value was derived from the slope of the conductance *versus* gap height plot (**Figure 1D**).

This latter point was found particularly crucial as it helped determining the presence of air entrapped within the porous structure. Strong deviation between both values (> 20 $\mu S \cdot cm^{-1}$) was a sign for air entrapment and the measurement was discarded. The presence of air had to be prevented as it was found to greatly affect all derived parameters conductance, $\zeta_{internal}$ and $\zeta_{external}$.

### *2.2.3 Measurement under different electrolyte solutions*

To gain understanding on the affinity of ions for hydroxyapatite and their effect on surface charge, streaming current measurements were performed using different electrolytes: phosphate buffered saline (GIBCO, 18912-014), calcium chloride ($CaCl_2 \cdot 2H_2O$, Sigma-Aldrich, C3881) and magnesium chloride ($MgCl_2 \cdot 6H_2O$, Panreac,131396) solutions. To facilitate comparison of the results and minimize variability between samples the same pair of samples was used to screen all electrolytes. Sample measurements started in 0.001 M KCl electrolyte with a conductivity of ~150 $\mu S \cdot cm^{-1}$. Samples were then rinsed with Milli Q water (18 $M\Omega \cdot cm$, Q-POD from Millipore) for at least 15 min before the new electrolyte was added. The concentration of each electrolyte was adjusted such that all measurements were performed at constant conductivity around 150 $\mu S \cdot cm^{-1}$. Once the electrolyte was introduced the samples were equilibrated for at least 15 min before any measurement was made.

## 3. RESULTS AND DISCUSSION

Preparation of hydroxyapatite bulk materials *via* biomimetic approaches is attracting great interest as it provides materials with close similarity, both in composition and structure, to the

mineral phase of bone. One such route is to use cementitious reactions involving the hydrolysis of alpha-tricalcium phosphate (α-TCP). In this specific context we prepared a series of substrates of identical composition, i.e. hydroxyapatite, but with different porosities.

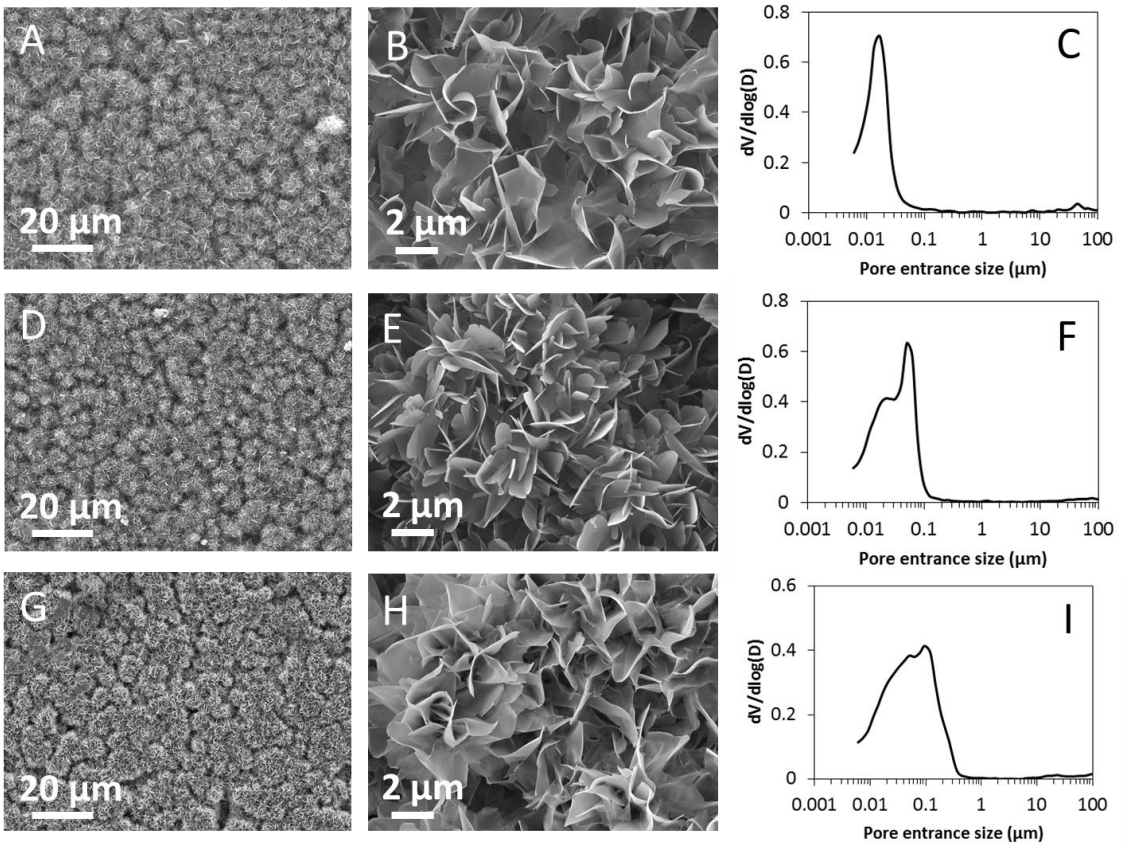


**Figure 2**: Surface microstructure and mercury intrusion porosimetry profiles for the various substrates prepared at the following L/P ratios: 0.35 (A-C), 0.45 (D-F) and 0.55 $mL \cdot g^{-1}$ (G-I). Note the close similarity in surface structure among materials despite differences in porosity content (~35, 45 and 50% for L/P 0.35, 0.45 and 0.55 respectively) and pore size distribution underneath the surface.

**Figure 2** shows three different hydroxyapatite substrates prepared using the following L/P ratios: 0.35, 0.45 and 0.55 $mL \cdot g^{-1}$. The surface morphology of all materials consisted of aggregates of plate-like crystals entangled together forming very similar surface morphologies.

Underneath the surface, however, aggregates would be more or less packed depending on the L/P ratio. This microstructure, typical of cements prepared by hydrolysis of α-TCP, is explained by the fact that hydrolysis takes place on the surface of each α-TCP particle. Thus, increasing the L/P ratio would only separate the different aggregates, yet each of them would still be composed of the typical plate-like crystals.[29] Mercury intrusion porosimetry curves are in good agreement with the trend observed for the different L/P ratios (**Figure 2**). The largest peak in the bimodal profiles corresponds to the channel-like network in between aggregates while the broader and smaller peak accounts for the pores between plate-like crystals. As the L/P ratio decreases, packing between aggregates increases and eventually the peak disappears if aggregates become too closely packed, i.e. for L/P 0.35. Even though differences in porosity and pore size distribution among L/P ratios were readily visible when analyzing the bulk sample, the surface morphology of the materials remained rather unaffected. This was probably an artifact of sample preparation during casting and spreading of the material in between the Teflon sheets.

We used these materials as a platform to investigate surface charge, which is a very relevant yet seldom reported property in bulk solid samples. Moreover, since porosity is key in the design of biomaterials this was taken the main focus of the present work.

### 3.1 Zeta potential of hydroxyapatite substrates with different porosities

As mentioned above, the recent work by Yaroshchuk and Luxbacher[20] has made possible to measure the surface charge of porous materials based on streaming current measurements at different gap heights (Eq. 3).[22,25,27] In their study the authors also stressed that for porous samples (with an open and hydraulically exposed pore structure) surface charge needs to be described in terms of an external and an internal zeta potential as was already discussed. The

former would describe the surface charge of the material surface itself and the latter the surface charge of the underlying pore structure (**Figure 3B**).

The complexity in the analysis of the surface charge of porous samples is easily understood from the measuring configuration (**Figure 3**). In tangential measurements samples are placed facing each other at a specific gap through which liquid is streamed. As already stated, when the sample is porous, part of the flow can go through the sample generating the so called "parasite current" that adds to the current along the gap. The measuring instrument, unable to separate both contributions, will only read a single current that will be the sum of the current generated along the gap and that within the porous sample. Thus, the resulting value for surface charge might become significantly distorted. On the other hand, isolation of the current inside the porous sample generates an internal zeta potential ($\zeta_{internal}$), which can have great impact in the interpretation of surface charge behavior in porous biomaterials (**Figure 3B**).

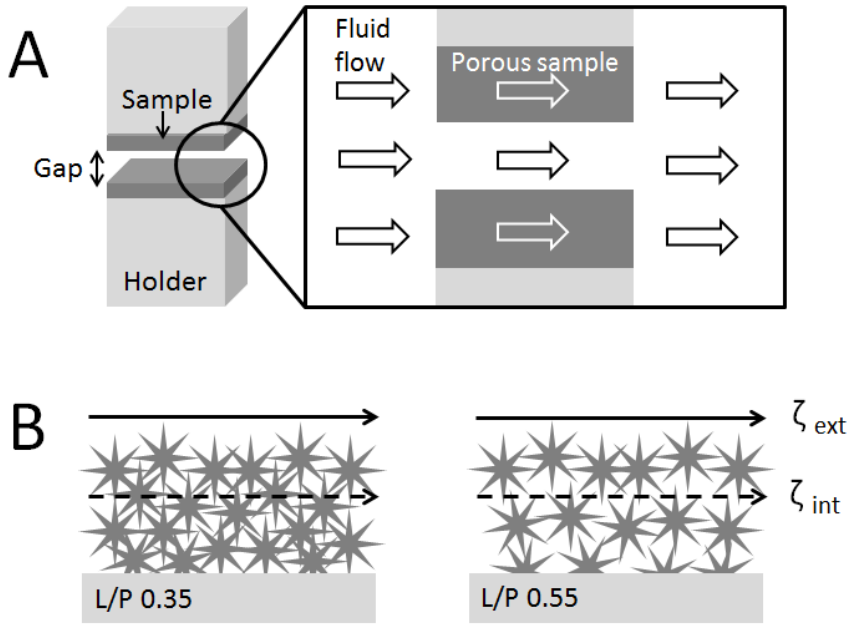

**Figure 3**: a) Sample configuration: samples glued in appropriate holders are placed facing each other at a specific gap height. During measurement, the fluid forced through the gap will travel along the channel but also through the samples provided they are porous. b) Sketch of the cross-section of samples prepared at two different liquid to powder ratios (L/P). Although the surface of both samples is identical, the cross-section reveals that low L/P yields denser samples than high L/P. Hydraulically exposed pores are responsible for the generation of an internal zeta potential ($\zeta_{internal}$) that represents the surface charge of the pore walls.

**Figure 4** summarizes the dependences of streaming current coefficient and cell electric conductance on channel height for all materials. Between three to five samples were measured at each condition to assess sample reproducibility. As was already predicted from Eq. 3, the dependences of streaming current coefficient ($dI_{str}/d\Delta p$) on channel height (H) are linear, which allows the accurate determination of the slope and intercepts thus, the calculation of the external and internal zeta potential, respectively. Similarly, from the linear dependence between the electric conductance inside the measuring cell and the gap height, one can estimate the conductance inside the pores (Cp). The measured conductance is composed of the conductance inside the streaming channel, which is determined by the electrical conductivity of the electrolyte ($\kappa_B$), and the conductance inside the pores (Cp). This latter value is obtained from the intercept of the plot, i.e. when the gap height equals to zero.

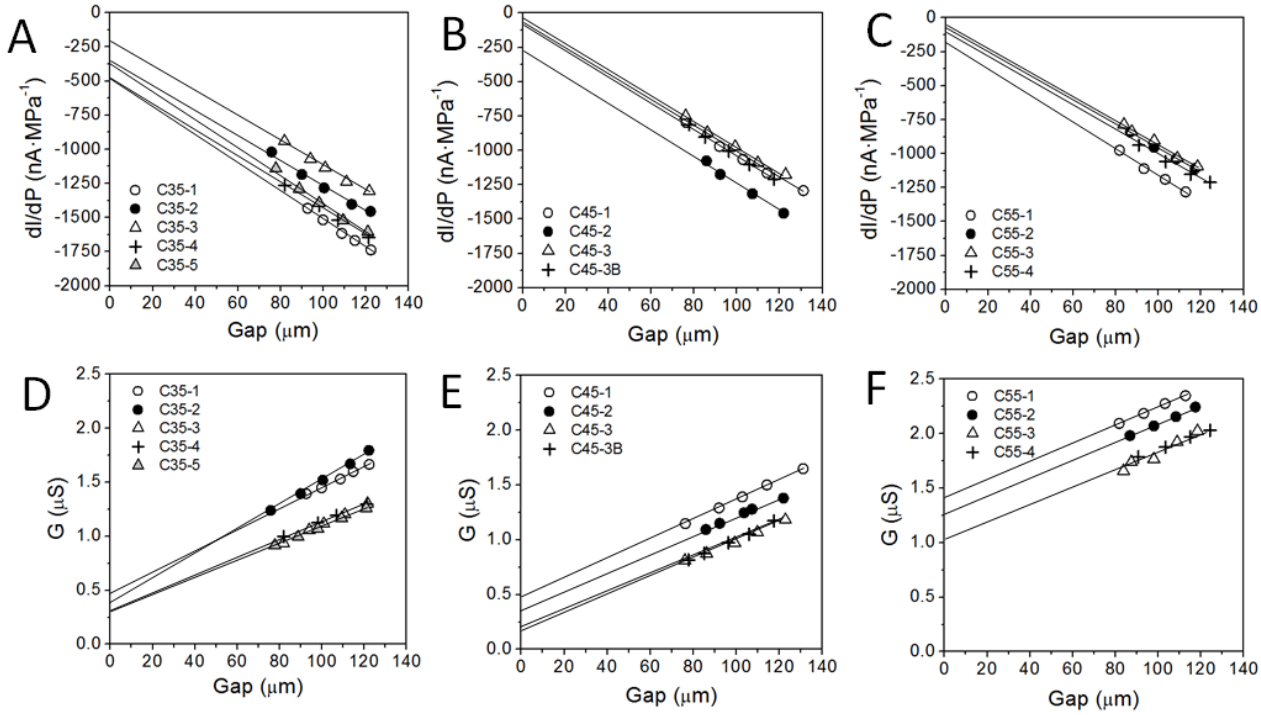


**Figure 4:** Streaming current coefficient and conductance dependence on gap height for the different samples: (A, D) for hydroxyapatite substrates prepared at the L/P ratio of 0.35, (B, E) L/P 0.45 and (C, F) L/P 0.55 $mL \cdot g^{-1}$. Numbers indicate different samples and letters account for the same sample measured after placing it on the sample holders in a different orientation.

There are interesting aspects worth to highlight from the various plots. On the one hand, the slope of all linear fits in the streaming current graphs look similar which allows predicting similar values in the external zeta potential regardless of L/P. In addition, it is observed that the offset value (intercept) never crosses zero, which evidences the presence of an additional streaming current flowing through the porous structure of the material. Interestingly, this value tends to increase with an increase in L/P (when comparing L/P 0.35 with 0.45 or 0.55 $mL \cdot g^{-1}$) which points to different behaviors between samples. Moreover, samples with L/P of 0.55 $mL \cdot g^{-1}$ clearly showed much higher pore conductance than L/P of 0.35 and 0.45 $mL \cdot g^{-1}$ which is

consistent with the higher porosity and larger pore size of the sample. The large dispersion between values possibly explains why there were no observable differences in conductance between 0.35 and 0.45 $mL \cdot g^{-1}$ samples despite the higher porosity and larger pore size of the latter.

Although with these plots we could readily calculate all parameters that control the surface charge of each sample, it is interesting to show first the zeta potential that would have been obtained assuming non-porous samples (Eq. 1), thus neglecting any current within the porous structure. For this particular case, zeta potential is obtained measuring the dependence of the streaming current with pressure for only one gap height typically around 100 μm (**Figure 5**). Even if there are not strong deviations between values, as all fall within -25 mV and -35 mV, the results seem to point that the denser the material is -especially for L/P 0.35 $mL \cdot g^{-1}$- the more negative the surface charge becomes. A result that is striking if one refers to the almost identical microstructures that were obtained for all substrates regardless of L/P (**Figure 2**).

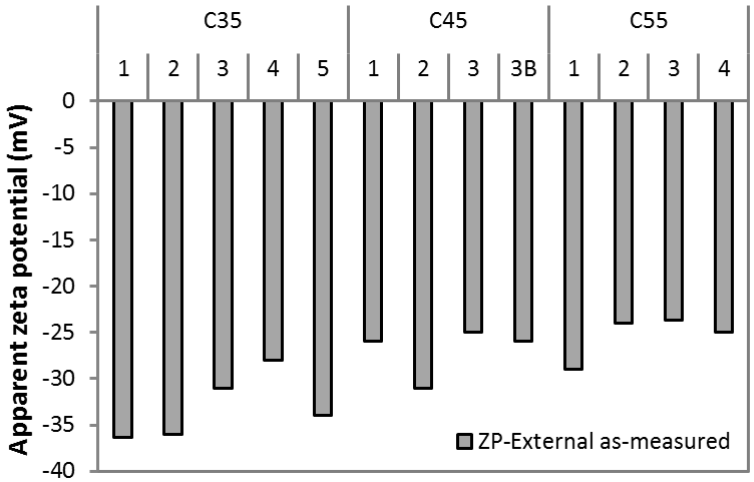


**Figure 5:** Surface charge determination of samples assuming they were non-porous. The measurement was performed from the dependence of the streaming current with pressure at a gap

of 100 μm. Numbers indicate different samples and letters account for the same sample measured after placing it on the sample holders in a different orientation.

Deriving now the results of the measurements performed at the different gap heights (Figure 4) we obtain the results displayed in Figure 6. The slope and offset of the linear fits (Figure 4) allow to separately determine the internal and external zeta potential, which provides a more coherent value in the external zeta potential for all samples. Indeed, the almost identical texture predicts a similar value, which is now obtained after correcting the values from the internal current flowing through the porous sample.

Values of zeta potential for HA are readily available from the literature but unfortunately there is a large variability which mainly arises from differences in measuring conditions (e.g. electrolyte composition, ionic strength or pH), different sample composition/structure and from different measuring configurations (e.g. values obtained from electrophoretic mobility measurements versus tangential/transversal streaming potential/current measurements).[30–34] In spite of the large variability, it has been gaining consensus that synthetic HA has an isoelectric point (IEP) between pH 5-7.[30,35] The sign of the zeta potential obtained in the present work is negative at pH 6 which is consistent with the IEP. The magnitude of ~-23 mV, however, differs among works. Since the surface charge of a mineral is determined by the concentration of the so-called "potential determining ions" in solution which, in the case of apatite are the lattice ions and their reaction products with water,[30] it is understandable that the synthesis route of HA and the measuring conditions (e.g. pH and electrolyte nature) would be critical dictating the materials' surface charge. In the present work the good agreement between the external morphology observed for all different cements -prepared using the same reagents and measured

under identical conditions- and the almost identical values in external zeta potential confirms the hypothesis that the contribution of the parasite current need to be removed to unveil the real value.

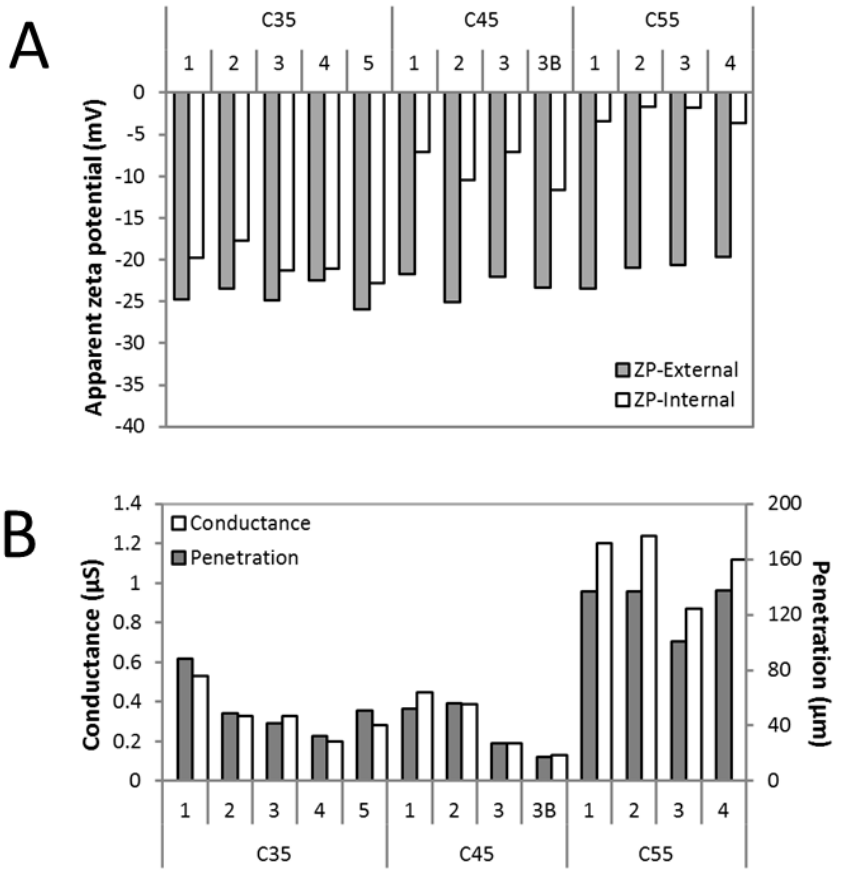


**Figure 6:** Values obtained for internal and external zeta potential (A), pore conductance and flow penetration within the samples (B) derived from the linear fits shown in Fig. 4 and Eq. 3 and 3. Numbers indicate different samples and letters account for the same sample measured after placing it on the sample holders in a different orientation.

Interestingly, the parasite current in the porous sample results in an internal zeta potential that changes depending on sample porosity (L/P). Since the structural unit in the building of cements can be seen as an aggregate of plate-like crystals (Figure 3B), and L/P only dictates the packing density of aggregates, it seems reasonable to ascribe the increase in internal zeta potential to porosity and pore size. With an increase in the liquid to powder ratio of the sample, the internal zeta potential becomes less negative.

It seems unreasonable to assume that higher porosity introduces a smaller contribution of streaming current inside pores. This assumption is in contradiction to the observed pore conductance and to the series of microfiltration membranes with uniform chemistry but increasing pore size reported by Yaroshchuk and Luxbacher.[20] We thus interpret the higher internal zeta potential for L/P 0.55 $mL \cdot g^{-1}$ by a difference in the ionic environment of superficial HA and HA inside pores. Inside the pores, ions released owing to partial dissolution of HA would become more concentrated in the interior of the sample than on the surface where ion diffusion/convection would more easily occur. This local high ionic strength would explain the reduction in the magnitude of the - still negative - zeta potential inside the pores. For materials with smaller interconnected porosity i.e., L/P 0.35 $mL \cdot g^{-1}$, the accessibility of the aqueous solution is limited to the near-surface porous structure and so the contribution of the interior becomes less obvious. When increasing L/P, permeation of liquid to the pore surface buried underneath the external cement surface reveals more strongly the differences in charging behavior.

One essential aspect related to the calculation of the internal zeta potential in Figure 6 was the estimation of current penetration within the samples. Indeed, the internal zeta potential is linked to the thickness of the sample penetrated by the current (*Hp* in Eq. 3). For highly porous

materials with well interconnected pores this refers to the full sample thickness, yet, for cements, even if they are porous, pore size is too small (**Figure 2**) to envisage full sample penetration.[29] Thus, flow penetration had to be estimated. This was done by making use of conductance analysis, in particular, of the conductivity reduction factor that relates to the material porosity (Eq. 4) as follows.[20,28]

$$\Upsilon = \frac{Cp}{\kappa_B \cdot \left(W \cdot \frac{A}{L}\right)} \qquad \text{Eq.4}$$

Where $\Upsilon$ represents the material porosity, Cp the conductance inside the pores, $\kappa_B$ the electrical conductivity of the aqueous solution, L the length of the sample and A the cross-section of the sample penetrated by the flow, i.e., A = W·Hp, were Hp is the penetrated depth.

Essentially this ratio (Eq. 4) relates the electrical conductance within the porous sample penetrated by the liquid, to that of an electrolyte solution of identical dimensions. Thus, the reduction in conductivity arises as the result of cement porosity and pore tortuosity. The possibility of determining the values of conductance inside the pores (**Figure 3**) together with the known values for sample porosity (**Figure 2**) allows easily estimating the penetration depth (Eq. 4). As expected, higher penetration depths occur for samples with larger interconnected pores and this is reflected in the higher pore conductance for L/P 0.55 $mL \cdot g^{-1}$.

Although the calculation of the flow penetration depth within the samples allows for a more reliable internal zeta potential determination, this value ($\zeta_{internal}$) should only be taken as apparent because of potential overlap of diffuse parts of the electric double layer inside the pores (the electric double layer is around 10 nm for a 0.001 M electrolyte composed of monovalent ions). In fact, Eq. 2 was derived assuming that both, the channel height and the pores of the sample are large with respect to the electric double layer. This condition is easily fulfilled in the channel gap where the 80-120 μm of gap height largely exceeds the few nanometers of the electric double

layer but may not necessarily be true inside the porous material depending on pore size. Thus, the internal zeta potential should be viewed as an apparent or approximate value. For the determination of the external zeta potential, since the gap height is large enough, no overlapping of the double layer occurs thus fulfilling the conditions for validity of the Helmholtz-Smoluchowski equation. Moreover, changes in the flow conditions inside the porous material when compared to that of the gap could also lead to changes in the magnitude of the calculated internal zeta potential -but not in the sign- reinforcing the "apparent" character of the internal zeta potential.

Taken together all these results, it is evident that streaming current measurements at different gap heights are essential for the accurate determination of the surface charge of porous materials. In addition to allowing the accurate determination of the external zeta potential of materials, the presented approach provides an internal zeta potential that estimates the surface charge of the pore walls underneath the surface. In the biomaterials field, where texture and porosity are widely used strategies to modify protein adsorption and cell behavior, the consideration of the effect of porosity on the determination of surface charge, can have great repercussion and deserves in-depth investigation.

### 3.2 Zeta potential of hydroxyapatite substrates in different electrolytes

In addition to texture, the chemistry of the material has commonly the greatest impact on surface charge. Hydroxyapatite, in particular biological apatite, is well known for its capacity to exchange surface ions with the surrounding fluids. In fact, its surface is considered as a reservoir for mineral ions that may entrap or release ions depending on biological demand.[36] This reactivity has been investigated in various fields for the removal of heavy metals from waste

water or soils,[37–39] as well as in biomedical applications for the activation of apatite surfaces through the selective exchange of surface calcium ions with biologically-active cations such as $Mg^{2+}$ or $Sr^{2+}$.[36,40]

The facile ionic exchanges that hydroxyapatite undergoes have essentially been explained by the existence of a metastable hydrated layer on the crystal surface containing loosely bound ions.[41] Recent works have put forward that through the presence of this layer, ionic exchanges become very fast and easy in addition of being reversible. [36,40]

The presence in the biological milieu of a wide range of ions and the inherent reactivity of hydroxyapatite surfaces for ions, questions the relevance of surface charge measurements performed in environments far from the physiological situation. In an attempt to prove ion adsorption selectivity, we have performed surface charge measurements using different electrolytes. Studies carried out on HA nanoparticles suspensions had shown a great effect depending on the type of ion.[30-31,35]

**Figure 7** summarizes the results performed on two different samples prepared at the L/P of 0.35 and 0.55, respectively. The various electrolytes used were phosphate buffered saline (PBS), calcium chloride and magnesium chloride salts. The concentration of the different salts was adjusted to maintain the conductivity of the electrolyte solution close to 150 $\mu S \cdot cm^{-1}$. The pH was kept around 6.0-7.3. As shown in **Figure 7**, PBS did not alter the surface charge values of the samples resulting in similar internal and external zeta potentials to those reported for conventional KCl electrolyte. Although it is well known that the divalent form of phosphate ions is involved in the hydrated layer,[42] the presence of other salts, namely NaCl and KCl, in the formulation of PBS could have hampered their interaction. In fact, in the formulation of the PBS tablets, sodium chloride was present at a concentration 14 times higher than that of phosphate

salts. Interestingly both, Ca and Mg electrolytes were observed to affect significantly the surface charge of the materials. The adsorption of the divalent cations on the crystal surface of hydroxyapatite caused a clear increase in the external zeta potential to around -10 mV regardless of the type of ion and substrate. The internal zeta potential, similarly to the trend already observed with KCl, varied depending on the material. For the more porous sample (with 50% porosity and pore conductance around 1 μS) the internal zeta potential was close to neutral while for the denser material (34% porosity and pore conductance around 0.25 μS) was kept rather close to the values of the external one.

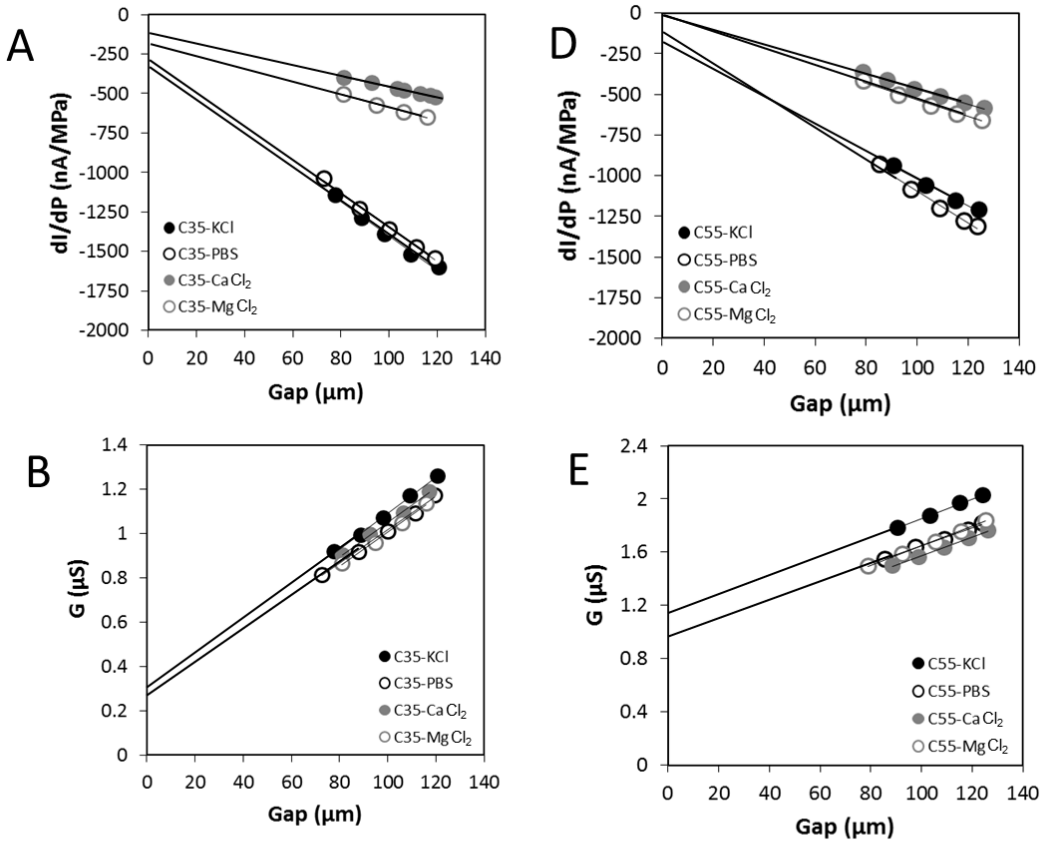


C

| C35 | ZP Ext, mV | ZP Int, mV | Cond. µS |
|---|---|---|---|
| KCl | -26.0 | -22.9 | 0.28 |
| PBS | -26.1 | -18.8 | 0.26 |
| $CaCl_2$ | -7.9 | -9.7 | 0.26 |
| $MgCl_2$ | -10.2 | -13.1 | 0.23 |

F

| C55 | ZP Ext, mV | ZP Int, mV | Cond. µS |
|---|---|---|---|
| KCl | -19.7 | -3.4 | 1.12 |
| PBS | -23.8 | -1.7 | 0.98 |
| $CaCl_2$ | -11.1 | -0.1 | 0.88 |
| $MgCl_2$ | -12.5 | -0.3 | 0.92 |

**Figure 7**: Streaming current and conductance dependence on gap height for two samples prepared with L/P of 0.35 (A-C) and 0.55 $mL \cdot g^{-1}$(D-F), respectively. Measurements were done using different electrolytes in the following order: KCl, PBS, $CaCl_2$ and $MgCl_2$. The slope and intercept values of the linear fits were used to compute the external and internal zeta potential shown in the tables. Pore conductance was obtained from the intercept of the linear fitting of cell conductance dependence with gap height.

One interesting fact that would deserve further investigation is whether Ca and Mg become incorporated in the hydrated layer of the crystals or they simply adsorb on the crystal surface without mediation of this layer. The reported behavior that ions once incorporated in the hydrated layer cannot be removed by dilution (they could however be exchanged by other divalent ions),[42] questions its presence in our studies. We have observed that after measuring the surface charge in $CaCl_2$ electrolyte if we rinse the samples with KCl (note that monovalent ions do not incorporate in the hydrated layer)[42] and measure the surface charge again, we could almost recover the values already obtained for KCl.

In spite of this latter issue that will need further investigation, it is clear that the presence of certain ions in the electrolyte, e.g. divalent cations, can significantly affect surface charge. Thus, even if the zeta potential of the materials have been accurately determined using KCl as electrolyte, the complex cocktail of ions in the biological milieu with potential affinity for hydroxyapatite need to be better understood to help predicting subsequent protein adsorption and cell behavior. Indeed, even if the nature of the adsorbed proteins is crucial for cell behavior, this is believed to be preceded by an interfacial water layer containing low molecular weight solutes such as ions and aminoacids.[43]

## 4. CONCLUSIONS

This work proves that streaming current measurements represent a very convenient way of determining the surface charge of bulk porous biomaterials. An internal and external zeta potential has been derived accounting for the surface charge of pore surface the former, and the surface charge of the materials surface the later. The similar surface morphology for all materials led to similar external zeta potential while the different degree in interconnected porosity in the bulk of the samples let to differences in internal zeta potential and pore conductance.

Additionally, studies with different electrolytes revealed strong affinity of divalent cations for hydroxyapatite, which greatly affected internal and external surface charge. This work thus put forward that both the materials topography and the choice of relevant electrolyte solutions need to be accounted in the analysis of the surface charge of biomaterials.

ACKNOWLEDGMENTS

Authors acknowledge the Spanish Government through Project MAT2012-38438-C03, co-funded by the EU through European Regional Development Funds as well as Marie Curie Actions FP7-PEOPLE-2011-COFUND (GROWTH 291795) via the VINNOVA programme Mobility for Growth (project n. 2013-01260). Support for the research of MPG was received through the ‘‘ICREA Academia’’ award for excellence in research, funded by the Generalitat de Catalunya. The authors also acknowledge Dr Elisabeth Engel and Dr Oscar Castaño from the Institute for Bioengineering of Catalonia for allowing us to use the Z-potential instrument.

REFERENCES

(1) Biggs, M. J. P.; Richards, R. G.; Dalby, M. J. Nanotopographical modification: A regulator of cellular function through focal adhesions. *Nanomedicine Nanotechnology, Biol. Med.* **2010**, *6* (5), 619–633.

(2) Chang, H.; Wang, Y. Cell responses to surface and architecture of tissue engineering scaffolds. *Regen. Med. Tissue Eng. - Cells Biomater.* **2011**, 569–588.

(3) Chen, C. S. Geometric Control of Cell Life and Death. *Science* **1997**, *276* (5317), 1425–1428.

(4) Dalby, M. J.; Gadegaard, N.; Riehle, M. O.; Wilkinson, C. D. W.; Curtis, A. S. G. Investigating filopodia sensing using arrays of defined nano-pits down to 35 nm diameter

in size. *Int. J. Biochem. Cell Biol.* **2004**, *36* (10), 2015–2025.

(5) Wilson, C. J.; Clegg, R. E.; Leavesley, D. I.; Pearcy, M. J. Mediation of biomaterial-cell interactions by adsorbed proteins: a review. *Tissue Eng.* **2005**, *11* (1-2), 1–18.

(6) Nakanishi, K.; Sakiyama, T.; Imamura, K. On the adsorption of proteins on solid surfaces, a common but very complicated phenomenon. *J. Biosci. Bioeng.* **2001**, *91* (3), 233–244.

(7) Lord, M. S.; Foss, M.; Besenbacher, F. Influence of nanoscale surface topography on protein adsorption and cellular response. *Nano Today* **2010**, *5* (1), 66–78.

(8) Kawasaki, T. Hydroxyapatite as a liquid chromatographic packing. *J. Chromatogr. A* **1991**, *544*, 147–184.

(9) Itagaki T, Yoshida M, Abe S, Omichi H, N. Y. Separation of human tear proteins with ceramic hydroxyapatite high-performance liquid chromatography. *J. Chromatogr.* **1993**, *620*, 149–152.

(10) Cummings LJ, Snyder MA, B. K. Protein chromatography on hydroxyapatite columns. *Methods Enzym.* **2009**, *463*, 387–404.

(11) Kandori, K.; Fudo, A.; Ishikawa, T. Study on the particle texture dependence of protein adsorption by using synthetic micrometer-sized calcium hydroxyapatite particles. *Colloids Surfaces B Biointerfaces* **2002**, *24* (2), 145–153.

(12) Zhuang, Z.; Aizawa, M. Protein adsorption on single-crystal hydroxyapatite particles with preferred orientation to a(b)- and c-axes. *J. Mater. Sci. Mater. Med.* **2013**, *24* (5), 1211–1216.

(13) Baxter, F. R.; Bowen, C. R.; Turner, I. G.; Dent, A. C. E. Electrically active bioceramics: a review of interfacial responses. *Ann. Biomed. Eng.* **2010**, *38* (6), 2079–2092.

(14) Kizuki, T.; Ohgaki, M.; Katsura, M.; Nakamura, S.; Hashimoto, K.; Toda, Y.; Udagawa, S.; Yamashita, K. Effect of bone-like layer growth from culture medium on adherence of osteoblast-like cells. *Biomaterials* **2003**, *24* (6), 941–947.

(15) Bodhak, S.; Bose, S.; Bandyopadhyay, A. Role of surface charge and wettability on early stage mineralization and bone cell-materials interactions of polarized hydroxyapatite. *Acta Biomater.* **2009**, *5* (6), 2178–2188.

(16) Ohgaki, M.; Kizuki, T.; Katsura, M.; Yamashita, K. Manipulation of selective cell adhesion and growth by surface charges of electrically polarized hydroxyapatite. *J. Biomed. Mater. Res.* **2001**, *57* (3), 366–373.

(17) Fröhlich, E. The role of surface charge in cellular uptake and cytotoxicity of medical nanoparticles. *Int. J. Nanomedicine* **2012**, *7*, 5577–5591.

(18) Chen, L.; Mccrate, J. M.; Lee, J. C.-M.; Li, H. The role of surface charge on the uptake and biocompatibility of hydroxyapatite nanoparticles with osteoblast cells. *Nanotechnology* **2011**, *22* (10), 1–20.

(19) Gratton, S. E. A; Ropp, P. A; Pohlhaus, P. D.; Luft, J. C.; Madden, V. J.; Napier, M. E.; DeSimone, J. M. The effect of particle design on cellular internalization pathways. *Proc. Natl. Acad. Sci. U. S. A.* **2008**, *105* (33), 11613–11618.

(20) Yaroshchuk, A.; Luxbacher, T. Interpretation of electrokinetic measurements with porous films: role of electric conductance and streaming current within porous structure. *Langmuir* **2010**, *26* (13), 10882–10889.

(21) Moritz, T.; Benfer, S.; Árki, P.; Tomandl, G. Influence of the surface charge on the permeate flux in the dead-end filtration with ceramic membranes. *Sep. Purif. Technol.* **2001**, *25* (1-3), 501–508.

(22) Déon, S.; Fievet, P.; Osman Doubad, C. Tangential streaming potential/current measurements for the characterization of composite membranes. *J. Memb. Sci.* **2012**, *423-424*, 413–421.

(23) Bukšek, H.; Luxbacher, T.; Petrinić, I. Zeta potential determination of polymeric materials using two differently designed measuring cells of an electrokinetic analyzer. *Acta Chim. Slov.* **2010**, *57* (3), 700–706.

(24) Fievet, P.; Sbaï, M.; Szymczyk, A.; Vidonne, A. Determining the ζ-potential of plane membranes from tangential streaming potential measurements: effect of the membrane body conductance. *J. Memb. Sci.* **2003**, *226* (1-2), 227–236.

(25) Xie, H.; Saito, T.; Hickner, M. A. Zeta potential of ion-conductive membranes by streaming current measurements. *Langmuir* **2011**, *27* (8), 4721–4727.

(26) Yaroshchuk, A.; Ribitsch, V. Role of Channel Wall Conductance in the Determination of -Potential from Electrokinetic Measurements. *Langmuir* **2002**, *18*, 2036–2038.

(27) Szymczyk, A.; Dirir, Y. I.; Picot, M.; Nicolas, I.; Barrière, F. Advanced electrokinetic characterization of composite porous membranes. *J. Memb. Sci.* **2013**, *429*, 44–51.

(28) Yaroshchuk, A.; Bernal, E. E. L.; Luxbacher, T. Electrokinetics in undeveloped flows. *J. Colloid Interface Sci.* **2013**, *410*, 195–201.

(29) Espanol, M.; Perez, R. a; Montufar, E. B.; Marichal, C.; Sacco, A.; Ginebra, M. P. Intrinsic porosity of calcium phosphate cements and its significance for drug delivery and tissue engineering applications. *Acta Biomater.* **2009**, *5* (7), 2752–2762.

(30) Wang, Y. H. C. In *Adsorption on and surface chemistry of hydroxyapatite*; Misra, D. N., Ed.; Plenum Publishing Corporation, 1984, 1984; pp 129–149.

(31) Somasundaran, P.; Agar, G. Further Streaming Potential Studies on Apatite in Inorganic Electrolytes.*Trans. SME AIME* **1972**, *252*, 348–352.

(32) Chen, L.; Mccrate, J. M.; Lee, J. C.-M.; Li, H. The role of surface charge on the uptake and biocompatibility of hydroxyapatite nanoparticles with osteoblast cells. *Nanotechnology* **2011**, *22* (10), 105708.

(33) Matsumura, H.; Kawasaki, K.; Okumura, N.; Kambara, M.; Norde, W. Characterization of the surface of protein-adsorbed dental materials by wetting and streaming potential measurements. *Colloids Surfaces B Biointerfaces* **2003**, *32* (2), 97–103.

(34) Jack, K. S.; Vizcarra, T. G.; Trau, M. Characterization and surface properties of amino-acid-modified carbonate-containing hydroxyapatite particles. *Langmuir* **2007**, *23* (24), 12233–12242.

(35) Harding, I. S.; Rashid, N.; Hing, K. A. Surface charge and the effect of excess calcium ions on the hydroxyapatite surface. *Biomaterials* **2005**, *26* (34), 6818–6826.

(36) Cazalbou, S.; Eichert, D.; Ranz, X.; Drouet, C.; Combes, C.; Harmand, M. F.; Rey, C. Ion exchanges in apatites for biomedical applications. *J Mat Sci Mat Med* **2005**, *16*, 405–409.

(37) Takashi Suzuki, Toshiaki Hatsushika, Y. H. Synthetic hydroxyapatites employed as inorganic cation-exchangers. *J. Chem. Soc., Faraday Trans.* **1981**, *77*, 1059–1062.

(38) Stötzel, C.; Müller, F. a; Reinert, F.; Niederdraenk, F.; Barralet, J. E.; Gbureck, U. Ion adsorption behaviour of hydroxyapatite with different crystallinities. *Colloids Surf. B. Biointerfaces* **2009**, *74* (1), 91–95.

(39) Chen, S. B.; Ma, Y. B.; Chen, L.; Xian, K. Adsorption of aqueous Cd 2+ , Pb 2+ , Cu 2+ ions by nano-hydroxyapatite: Single- and multi-metal competitive adsorption study. *Geochem. J.* **2010**, *44*, 233–239.

(40) Drouet, C.; Carayon, M.-T.; Combes, C.; Rey, C. Surface enrichment of biomimetic apatites with biologically-active ions Mg2+ and Sr2+: A preamble to the activation of bone repair materials. *Mater. Sci. Eng. C* **2008**, *28* (8), 1544–1550.

(41) Rey, C.; Hina, A.; Tofighi, A.; Glimcher, M. Maturation of poorly crystalline apatites: Chemical and structural aspects in vivo and in vitro. *CELLS Mater.* **1995**, *5*, 345–356.

(42) Rey, C.; Combes, C.; Drouet, C.; Sfihi, H.; Barroug, A. Physico-chemical properties of nanocrystalline apatites: Implications for biominerals and biomaterials. *Mater. Sci. Eng. C* **2007**, *27* (2), 198–205.

(43) Vogler, E. A. Water and the acute biological response to surfaces. *J. Biomater. Sci. Polymer Edn.*, 1999, *10*, 1015–1045.